

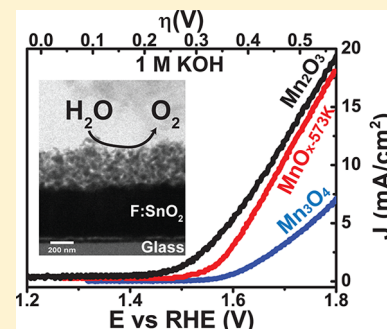
Evaluation of MnO_x , Mn_2O_3 , and Mn_3O_4 Electrodeposited Films for the Oxygen Evolution Reaction of Water

Alejandra Ramírez,* Philipp Hillebrand, Diana Stellmach, Matthias M. May, Peter Bogdanoff, and Sebastian Fiechter*

Helmholtz-Zentrum Berlin für Materialien und Energie, Institute for Solar Fuels, Hahn-Meitner-Platz 1, 14109 Berlin, Germany

S Supporting Information

ABSTRACT: Different manganese oxide phases were prepared as thin films to elucidate their structure–function relationship with respect to oxygen evolution in the process of water splitting. For this purpose, amorphous MnO_x films anodically deposited on F:SnO₂/glass and annealed at different temperatures (to improve film adherence and crystallinity) were tested in neutral and alkaline electrolytes. Differential electrochemical mass spectroscopy showed that the anodic current correlated well with the onset of the expected oxygen evolution, where in 1 M KOH, the anodic current of crystalline α -Mn₂O₃ films was determined to onset at an overpotential (η) of 170 mV_{RHE} (at $J = 0.1 \text{ mA/cm}^2$) with current densities of ca. 20 mA/cm² at $\eta = 570 \text{ mV}_{\text{RHE}}$. Amorphous MnO_x films heated at 573 K (MnO_x -573 K) were found to improve their adherence to F:SnO₂/glass substrate after heat treatment with a slight crystallization detected by Raman spectroscopy. The onset of water oxidation of MnO_x -573 K films was identified at $\eta = 230 \text{ mV}_{\text{RHE}}$ (at $J = 0.1 \text{ mA/cm}^2$) with current densities of ca. 20 mA/cm² at $\eta = 570 \text{ mV}_{\text{RHE}}$ (1 M KOH). The least active of the investigated manganese oxides was Mn_3O_4 with an onset at $\eta = 290 \text{ mV}_{\text{RHE}}$ (at $J = 0.1 \text{ mA/cm}^2$) and current densities of ca. 10 mA/cm² at $\eta = 570 \text{ mV}_{\text{RHE}}$ (1 M KOH). In neutral solution (1 M KPi), a similar tendency was observed with the lowest overpotential found for α -Mn₂O₃ followed by MnO_x -573 K and Mn_3O_4 . X-ray photoelectron spectroscopy revealed that after electrochemical treatment, the surfaces of the manganese oxide electrodes exhibited oxidation of Mn II and Mn III toward Mn IV under oxygen evolving conditions. In the case of α -Mn₂O₃ and MnO_x -573 K, the manganese oxidation was found to be reversible in KPi when switching the potential above and below the oxygen evolution reaction (OER) threshold potential. Furthermore, scanning electron microscopy (SEM) images displayed the presence of an amorphous phase on top of all manganese oxide films here tested after oxygen evolution. The results indicate that structural changes played an important role in the catalytic activity of the manganese oxides, in addition to oxidation states, a large variety of Mn–O bond lengths and a high concentration of oxygen point defects. Thus, compared to Mn_3O_4 , crystalline α -Mn₂O₃ and MnO_x -573 K are the most efficient catalyst for water oxidation in the manganese–oxygen system.



1. INTRODUCTION

To generate hydrogen by water splitting using inexpensive photovoltaic (PV) hybrid electrolyzers with enhanced efficiency, the development of earth abundant catalysts is in demand.^{1,2} Such process is successfully performed by nature using enzyme systems of high complexity in photosystem I and II capable to oxidize water into oxygen.^{3,4} The “photosystem II” contains an active manganese cluster, which efficiently manages the four-electron transfer for the oxidation of water (OER) to oxygen.⁵ Thus, the investigation of manganese-based materials is of interest to mimic such an efficient process. Manganese oxides are low-cost, earth abundant, and widely utilized as cathode materials in aqueous and nonaqueous batteries.^{6–8} In addition, they are also well-known as electrochemical capacitors,^{9–13} chemical and water oxidation catalysts^{1,14–23} and oxygen reduction catalysts.^{24,25} The reported electrochemical studies on manganese oxides (electrochemically deposited) demonstrated that in the anodic region α -Mn₂O₃ on glassy carbon (0.1 M KOH)¹⁸ and MnO_x deposited on Au or Pt (0.5 M KOH)²⁰ were capable to produce currents above

10 mA/cm² at 1.8 V vs RHE, which were attributed to the oxygen generation. Recently, amorphous films of MnO_x heated $\leq 393 \text{ K}$ were also observed to be active in 1 M NaOH showing currents above 10 mA/cm².²⁶ In the case of Mn_3O_4 , several authors reported oxygen evolution for powders, in clusters on mesoporous silica or as a cocatalysts in CoSe; nevertheless, systematic electrochemical investigations on OER thin films deposited on a conductive substrate were not yet performed. Catalysts prepared as thin films are in demand for future applications in solar-water splitting cells,² since the reduced thickness overcomes the limiting and frequently poor conductivity of some of the oxides.⁸ Among these preparation techniques, anodic deposition is a simple, low-cost technique, which can deposit homogeneous and thin manganese oxide films on a conductive substrate.^{10,27} In all described procedures at neutral conditions, the synthesis of a nearly amorphous phase

Received: January 27, 2014

Revised: June 3, 2014

Published: June 13, 2014

of manganese oxide was reported.^{9–12,27} In accordance to the phase transformations observed by Chen et al.,²⁸ the pristine electrochemically deposited manganese oxide crystallized by annealing to $\alpha\text{-Mn}_2\text{O}_3$ under air atmosphere at 773 K, and under nitrogen at 873 K to Mn_3O_4 . $\alpha\text{-Mn}_2\text{O}_3$ possesses a complex orthorhombic crystal structure (space group, *Pcab*)²⁹ with Mn^{3+} atoms octahedrally coordinated by oxygen, but differently distorted $[\text{MnO}_6]$ octahedra sharing edges and corners similar to the cubic mineral bixbyite $(\text{Fe}_{x}\text{Mn}_{1-x})_2\text{O}_3$,^{30–32} Mn_3O_4 with a tetragonal symmetry and a distorted spinel structure (space group, *I4_1/amd*) with Mn^{3+} ions located in weakly distorted octahedral sites $[\text{MnO}_6]$ and Mn^{2+} ions situated in tetrahedral sites $[\text{MnO}_4]$ is also known as the mineral hausmannite.^{33,34}

Based on already published electrochemical studies on manganese oxides,^{1,18,20} the present contribution investigated the stability of electrochemically deposited thin layers of manganese oxides on conductive glass in 1 M K_2PO_4 (neutral solution) and 1 M KOH (alkaline solution) and their oxygen evolution ability after heat treatment by cyclic voltammetry (CV) coupled with differential electrochemical mass spectroscopy (DEMS). Furthermore, all films were characterized using X-ray diffraction (XRD), Raman spectroscopy, transmission electron microscopy (TEM) and X-ray photoelectron spectroscopy (XPS).

2. EXPERIMENTAL SECTION

Materials. All materials were used as received. Na_2SO_4 (98%), KH_2PO_4 (99%), and K_2HPO_4 (99%), and 1 M KOH solution were purchased from Sigma-Aldrich, and $\text{MnSO}_4 \cdot \text{H}_2\text{O}$ (98 +%) was obtained from Merck. Conductive glass (F: SnO_2 /glass, TEC 7) from Pilkington (substrate) was previously cleaned inside an ultrasonic bath in ethanol (Sigma-Aldrich 98%) for 10 min. The substrate was then dried and weighted before and after film deposition.

Film Preparation. Films were prepared by galvanostatic deposition onto F: SnO_2 /glass ($1 \times 1.5 \text{ cm}^2$) at a current density of 0.25 mA/cm^2 in a three-electrode arrangement.^{27,35} The deposition cell consisted of a commercial platinum electrode as counter electrode, $\text{Hg}/\text{Hg}_2\text{SO}_4$ (+ 0.654 V vs NHE) as reference electrode and F: SnO_2 /glass as working electrode. Electrochemical deposition was carried out in a N_2 purged homogeneous solution of 0.25 M MnSO_4 and 0.25 M Na_2SO_4 (1:1 ratio) for 25 min. The films were then rinsed thoroughly with demineralized water and dried under air at 373 K (MnO_x -373 K). Further heating at 573 K, 773 K up to 1 h under air and at 873 K up to 3 h under nitrogen atmosphere was performed in order to obtain MnO_x -573 K and the desired crystalline phases $\alpha\text{-Mn}_2\text{O}_3$ and Mn_3O_4 .

Cyclic Voltammetry. Electrochemical evaluation was performed using CV in a three-electrode arrangement controlled by a Heka potentiostat/galvanostat. The cell consisted of a reference electrode (RE) of Ag/AgCl (+ 0.199 V vs NHE) for neutral solution and Hg/HgO (+ 0.132 V vs NHE) for alkaline solution, a counter electrode (CE) made of platinum wire, and a working electrode (WE) of the manganese oxide film deposited on the F: SnO_2 /glass. Films were cycled at room temperature in N_2 purged electrolyte with a sweep rate of 2 mV/s from 1.2 to 1.8 V vs RHE. Capacity behavior of the films was also evaluated using a three-electrode arrangement in neutral solution of 1 M KH_2PO_4 (KPi) with sweep rates between 5–100 mV/s from approximately 0.9 to 1.3 V vs RHE. RHE calculation was made using the formula $E_{\text{RHE}} = E_{\text{measured}} +$

$E_{\text{Ag}/\text{AgCl}} + 0.059p\text{H}$ where E_{measured} is the experimental potential, $E_{\text{Ag}/\text{AgCl}}$ reference electrode (+ 0.199 V) and pH of the electrolyte solution. Overpotential (η) was calculated using the formula $\eta = E_{\text{measured}} - 1.23$. Current densities were calculated using geometric surface areas. Potentiostatic measurements were performed using a VersaSTAT potentiometer in a three-electrode arrangement using Ag/AgCl as the reference and platinum wire as the counter electrode at 1.7 V vs RHE. In order to avoid oxygen saturation in the film, the electrolyte was constantly purged with N_2 gas during the measurement.

Differential Electrochemical Mass Spectroscopy.

DEMS was designed to simultaneously measure released gases during an electrochemical measurement. Detailed information about this system is given elsewhere.^{36,37} This equipment consisted of an inlet system between an electrochemical cell (three-electrode for CV conditions) and a differentially pumped vacuum system attached to a mass spectrometer (Balzers; QMI 420, QME 125, QMA 125 with 90° off axis Secondary Electron Multiplier). The inlet system was made of a porous hydrophobic membrane directly in contact with the working electrode (Supporting Information (SI), Figure S1). The oxygen generated at the working electrode diffused through the remaining thin layer of electrolyte toward the membrane. To some extent, the oxygen gas crossed the membrane, where it was simultaneously measured by the mass spectrometer during the electrochemical measurement (CV conditions).

Structural Characterization. XRD patterns of the films were recorded at room temperature on a D8-Advanced Bruker diffractometer with a $\text{Cu}-\text{K}\alpha$ ($\lambda = 1.54 \text{ \AA}$) source in Bragg–Brentano geometry using a Sol-X energy dispersive detector. Powder diffractograms were taken in an angle range from 20° to 60° using a step size of 0.02°/s and a step time of 4 s. Raman spectra up to 900 cm^{-1} were acquired at room temperature with a LabRam spectrometer (Horiba Jobin Yvon), integration time: 150 s. per spectrum, microscope objective: 100x, He/Ne laser (632.8 nm) as excitation source and a charge-coupled device (CCD) detector. Additional parts were an optical microscope (Olympus BX) to focus the surface of the sample, notch filter (D1.0) and a monochromator to separate Raman and Rayleigh scattering. Calibration was performed using a silicon wafer (phonon line at about 520 cm^{-1}). Cross-section images of the films were captured using a TEM (Philips CM12) with a LaB_6 cathode at 120 kV (acceleration voltage). Scanning electron microscopy (SEM) images were acquired using a LEO 1530 at 12 kV and 100 000x. XPS measurements were performed using a Specs system with a magnesium X-ray source. Samples were placed in a molybdenum sample holder and contacted with silver paste (Electrolit). Moreover, the spectra were fitted using Unifit 2011, where the C 1s peak at 284.5 eV was used to calibrate the spectra.

3. RESULTS AND DISCUSSION

Closed and homogeneous films were successfully electrodeposited on F: SnO_2 /glass and dried at 373 K with film thickness of approximately 650 nm (MnO_x -373 K) measured by cross-section TEM. The XRD patterns of the as-deposited MnO_x -373 K films revealed a nearly amorphous material with very weak reflections not visible in the presence of F: SnO_2 /glass (Figure 1a).^{11,12,38} The amorphous films were previously reported by our group without substrate, where a broad single reflection peak at $2\theta \sim 37^\circ$ was detected.³⁵ Heating these films at 573 K under air showed no increase in crystallinity (Figure

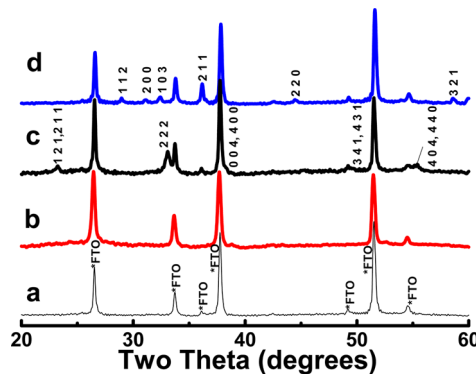


Figure 1. X-ray diffraction patterns of MnO_x -373 K (a), MnO_x -573 K (b), $\alpha\text{-Mn}_2\text{O}_3$ (c), and Mn_3O_4 (d) films deposited on $\text{F:SnO}_2/\text{glass}$.

1b), while when heated at 773 K under air led to a material that displayed intense crystalline reflections assigned to the $\alpha\text{-Mn}_2\text{O}_3$ crystal structure (Figure 1c) similar to a distorted bixbyite (JCPDS 73-1826). Moreover, films heated at 873 K under nitrogen crystallized into the Mn_3O_4 crystal structure (Figure 1d) addressed as the mineral hausmannite (JCPDS 18-0803). A slight displacement in 2θ of 0.63% and 0.21% (toward high values) was observed for $\alpha\text{-Mn}_2\text{O}_3$ and Mn_3O_4 , respectively. Such displacement was tentatively related to the presence of oxygen point defects in the films.³⁹

A thin film of sputtered RuO_2 deposited on titanium metal (reference electrode for oxygen evolution reaction) was identified as pure RuO_2 (JCPDS 40-1290) (SI, Figure S2). In accordance with the XRD data, TEM images also revealed structural differences (SI, Figure S3), where MnO_x -373 K exhibited a disordered arrangement and $\alpha\text{-Mn}_2\text{O}_3$ as well as Mn_3O_4 samples consisted of small crystallites of ca. 30 and 45–50 nm, respectively. Film thicknesses of the annealed films were observed to slightly expand for $\alpha\text{-Mn}_2\text{O}_3$ (750 nm) and to decrease for Mn_3O_4 (370 nm). Moreover, estimated from cross section TEM pictures (SI, Figure S3), MnO_x -373 K and $\alpha\text{-Mn}_2\text{O}_3$ films showed a higher porosity ($\sim 70 \text{ m}^2/\text{g}$) than Mn_3O_4 films ($\sim 25 \text{ m}^2/\text{g}$). SEM images of the MnO_x -573 K, $\alpha\text{-Mn}_2\text{O}_3$ and Mn_3O_4 films before and after electrochemistry (Figure 2) revealed changes in the surface morphology caused by the generation of an amorphous phase on top of the oxides as reported by several authors.^{40,41} In the case of MnO_x -373 K, SEM images after OER were not acquired due to the instability of the films.

Raman spectra in the 250–900 cm^{-1} region were acquired for all films (SI, Figure S4). MnO_x -373 K, MnO_x -573 K, $\alpha\text{-Mn}_2\text{O}_3$, and Mn_3O_4 films exhibited a common spectral feature typical for all manganese oxides, where a strong phonon band in the 640–660 cm^{-1} region and weak phonon bands in the range from 200 to 480 cm^{-1} were found.⁴² Changes in crystallinity were also detected by the presence of broader bands for amorphous phases than for crystalline phases.⁴³ The phonon band with large scattering intensity in the range from 640–660 cm^{-1} and a weak band at 732 cm^{-1} were assigned to A_{1g} spectroscopic species with symmetric vibrations $\nu_2(\text{Mn}-\text{O})$ and $\nu_1(\text{Mn}-\text{O})$, respectively.^{42,44} Moreover, the weak phonon band in the range from 480–460 cm^{-1} was attributed to the symmetric vibration $\nu_3(\text{Mn}-\text{O})$ ⁴⁵ and the weak bands at about 370–280 cm^{-1} to $\text{Mn}-\text{O}$ bending vibrations.^{42,45} Most of the vibrations found in these spectra were related to the motion of the oxygen atoms within the MnO_6 octahedral units in MnO_x -373 K, MnO_x -573 K, $\alpha\text{-Mn}_2\text{O}_3$ and Mn_3O_4 .⁴² While X-ray

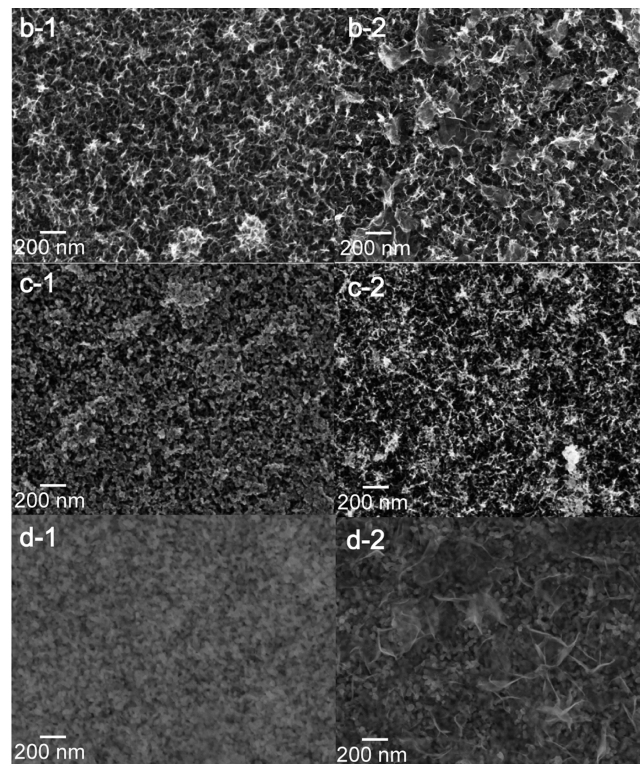


Figure 2. SEM images at room temperature (1) and after OER in 1 M KPi (2) of MnO_x -373 K, MnO_x -573 K (b), $\alpha\text{-Mn}_2\text{O}_3$ (c) and Mn_3O_4 (d) films deposited on $\text{F:SnO}_2/\text{glass}$.

diffraction of MnO_x -373 K and MnO_x -573 K films (Figure 1a,b) showed the presence of amorphous material (documented by a broad XRD peak at $2\theta = 37^\circ$), making small structural changes difficult to identify, the Raman spectra allowed us to further characterize the structural features of the deposited and annealed oxides, where a shift in the MnO_x -373 K strong phonon line at 649 cm^{-1} for up to 5 cm^{-1} was attributed to induced crystallinity changes after heat treatment at 573 K.⁴⁶ Furthermore, compared to the vibration modes reported by Julien et al.,⁴⁵ the structure of MnO_x -373 K and MnO_x -573 K were closer to that of $\beta\text{-MnO}_2$ (cassiterite structure), than the layer type oxides such as $\gamma\text{-MnO}_2$ or MnOOH (pyrolusite structure). The main difference to $\beta\text{-MnO}_2$ was the position of the A_{1g} vibration mode at 667 cm^{-1} , where for MnO_x -373 K was located at 649 cm^{-1} and for MnO_x -573 K at 644 cm^{-1} . Comparing these values with the Mn–O distances from crystal structures of different manganese oxides (Table S1), the Mn–O distance in MnO_x -373 K and MnO_x -573 K Mn were probably smaller than $\beta\text{-MnO}_2$ (1.88 Å) and similar to the mean Mn–O distance in Mn_3O_4 of 2.08 Å and $\alpha\text{-Mn}_2\text{O}_3$ of 2.04 Å.

Capacity evaluation of manganese oxides (SI, Figure S5 – S8) in 1 M KPi revealed a stable capacitive behavior in all films and showed no additional redox peaks. Capacity values calculated from CV curves were 24.71 mF/cm^2 for MnO_x -373 K and 49.23 mF/cm^2 for MnO_x -573 K. In the case of $\alpha\text{-Mn}_2\text{O}_3$ and Mn_3O_4 , the crystalline films displayed values of 12.79 mF/cm^2 and 1.73 mF/cm^2 , respectively. In general, the capacity of the electrodes decreased with increasing particle size (low surface area) as determined for MnO_x -373 K, $\alpha\text{-Mn}_2\text{O}_3$, and Mn_3O_4 by cross-section TEM, where MnO_x -373 K and $\alpha\text{-Mn}_2\text{O}_3$ displayed an estimated surface area of about 70 m^2/g .

and Mn_3O_4 displayed a value of about $25 \text{ m}^2/\text{g}$. However, besides the diminished surface area, the different specific capacities of the different electrode materials had to be considered. Compared to MnO_x -373 K, the significantly higher capacity found in MnO_x -573 K was related to changes in the surface composition detected by XPS (Figures 5 and 6) possibly due to a transition from amorphous to slightly improved crystallinity as identified by a 5 cm^{-1} Raman shift (SI, Figure S4). Preliminary results, which compared dense sputtered $\alpha\text{-Mn}_2\text{O}_3$ films (work to be published) with porous electrodeposited $\alpha\text{-Mn}_2\text{O}_3$ layers displayed similar current density values in KPi ($\eta = 270 \text{ mV}_{\text{RHE}}$ (at $J = 0.1 \text{ mA}/\text{cm}^2$) and current density ca. $10 \text{ mA}/\text{cm}^2$ at $\eta = 570 \text{ mV}_{\text{RHE}}$; thus, leading us to conclude that porosity had no major influence in this work since the depth (bulk) of the highly porous electrodes probably had only marginal presence in the OER due to a limited diffusion of protons and oxygen gas.

At positive potentials, up to 1.8 V vs RHE, all films exhibited significant anodic currents, which could be due to oxidation of the manganese oxides or electrooxidation of water to oxygen. In order to distinguish between these two possible processes, DEMS measurements were performed at a sweep rate of $2 \text{ mV}/\text{s}$ in neutral and alkaline solutions (Figures 3 and 4). These

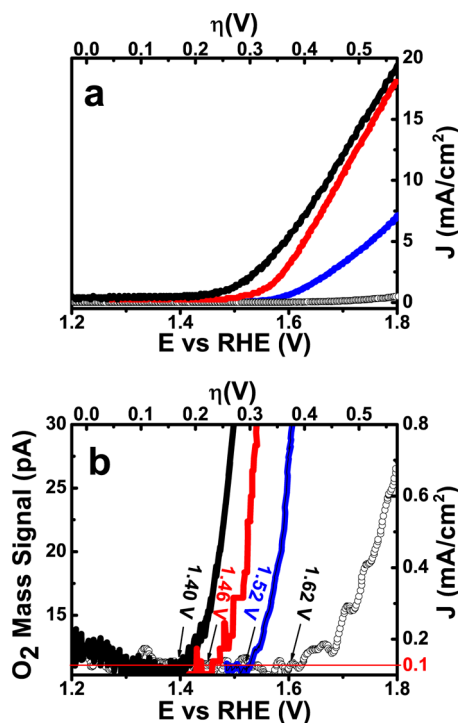


Figure 3. (a) Current density (J) and (b) oxygen mass signal (at low J) as a function of E vs RHE of MnO_x -573 K (red), $\alpha\text{-Mn}_2\text{O}_3$ (black) and Mn_3O_4 (blue) films deposited on $\text{F:SnO}_2/\text{glass}$ ($-O-$) in 1 M KOH.

measurements revealed that with increasing positive potential, first a low current was observed, which was not correlated to oxygen evolution. This potential range is given in Table S1 for all samples as preoxidation. It was assumed that these currents were involved in an oxidation process of the electrode interface (SI, Figures S9 and S10).^{10,47} At higher positive potential, the current started to increase exponentially, which was directly correlated to the mass signal of oxygen. The onset potential of this water oxidation reaction is depicted in Table S1.

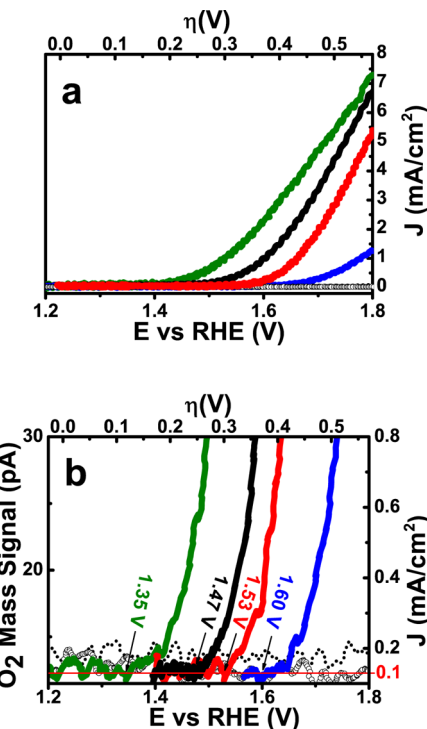


Figure 4. (a) Current density (J) and (b) oxygen mass signal (at low J) as a function of E vs RHE of sputtered RuO_2 (green), MnO_x -373 K (dotted lines), MnO_x -573 K (red), $\alpha\text{-Mn}_2\text{O}_3$ (black), and Mn_3O_4 (blue) films deposited on $\text{F:SnO}_2/\text{glass}$ ($-O-$) in 1 M KPi.

Amorphous MnO_x -373 K displayed preoxidation, and a significant onset potential was not reached before the sample started to peel off the substrate. Such mechanical detachment of the film was observed to occur when oxygen bubbles were generated from the substrate ($\text{F:SnO}_2/\text{glass}$) at potentials higher than 1.8 V vs RHE. In the case of MnO_x -573 K, $\alpha\text{-Mn}_2\text{O}_3$, and Mn_3O_4 , further increase in positive potentials displayed an exponential raise in the anodic current (J) and a significant oxygen signal (OE) (Table S1), which was well correlated to the observed current voltage diagrams (Figures 3 and 4). In alkaline solution, $\alpha\text{-Mn}_2\text{O}_3$ films were determined to onset at an overpotential (η) of $170 \text{ mV}_{\text{RHE}}$ ($J = 0.1 \text{ mA}/\text{cm}^2$) and exhibited current densities of ca. $20 \text{ mA}/\text{cm}^2$ at $\eta = 570 \text{ mV}_{\text{RHE}}$. The as-deposited MnO_x films heated at 573 K (MnO_x -573 K) were found to improve the adherence to the substrate after heat treatment; however, a slight crystallinity was observed by Raman spectroscopy. The onset of water oxidation of MnO_x -573 K films was identified at $\eta = 230 \text{ mV}_{\text{RHE}}$ ($J = 0.1 \text{ mA}/\text{cm}^2$) with current densities of ca. $20 \text{ mA}/\text{cm}^2$ at $\eta = 570 \text{ mV}_{\text{RHE}}$. The least active manganese oxide here studied was Mn_3O_4 with an onset at $\eta = 290 \text{ mV}_{\text{RHE}}$ ($J = 0.1 \text{ mA}/\text{cm}^2$) and a current density of ca. $10 \text{ mA}/\text{cm}^2$ at $\eta = 570 \text{ mV}_{\text{RHE}}$ (1 M KOH). In neutral solution (1 M KPi), a similar tendency was observed, where compared to the sputtered RuO_2 electrode with $\eta = 120 \text{ mV}_{\text{RHE}}$ ($J = 0.1 \text{ mA}/\text{cm}^2$) and current densities of ca. $10 \text{ mA}/\text{cm}^2$ at $\eta = 570 \text{ mV}_{\text{RHE}}$, $\alpha\text{-Mn}_2\text{O}_3$ and MnO_x -573 K electrodes displayed closer onset values and higher current densities than Mn_3O_4 .

The stability of the films was evaluated at a constant potential (1.7 V vs RHE) for 1 h in neutral and alkaline solution (SI, Figure S12–S13). In neutral solution, all samples initially displayed a fast degradation of the current followed by a slow process after ca. 30 min (SI, Figure S12). In alkaline solution, a

better stability was observed for all samples; however, a different degradation was noticed for MnO_x -573 K and Mn_3O_4 following a linear behavior. Surprisingly, $\alpha\text{-Mn}_2\text{O}_3$ showed less stability in KOH, where a faster degradation than in MnO_x -573 K and Mn_3O_4 was observed (SI, Figure S13). The reason for this different behavior is not clarified at the moment. The fast decrease in neutral solution could be related to the presence of a Mn-phosphate layer formed at the surface, which is known as a compound of low solubility. Such layer probably acted as a nonconductive barrier leading to a gradually decrease of current with increasing layer thickness. Further analyses need to be carried out in order to verify these hypotheses.

XP spectra of the Mn 2p, and O 1s region were measured to gain insight into the manganese oxidation states at the surface before and after cycling of the electrodes in the voltage range from 1.10 to 1.9 V vs RHE in neutral and alkaline solution (Table S2). The manganese valence was determined by the position of the multiplet splitting of Mn 2p, where in accordance with other authors,^{13,48–56} the position of Mn 2p_{3/2} was assigned to Mn IV (641.85–643.0 eV), Mn III (641.40–641.90 eV), and Mn II (640.10–641.12 eV). Moreover, the O 1s peak was attributed to the presence of Mn–O–Mn (529.3–530.3 eV), Mn–OH (530.5–531.5 eV), and H–O–H (531.8–532.8 eV).^{17,52,57,58} The XP spectrum of MnO_x -373 K revealed the Mn 2p transitions at 642.2 eV (Mn 2p_{3/2}) and 653.8 eV (Mn 2p_{1/2}), where the deconvoluted Mn 2p_{3/2} peak exhibited the presence of Mn IV (642.9 eV), Mn III (641.7 eV), and a small shoulder at 640.8 eV assigned to Mn II (Figure 5a). However, further evaluation after OER was not

increase in oxidation of the manganese atoms Mn III and Mn IV. A thermal treatment at higher temperatures evoked an increase in Mn IV. After OER in 1 M KPi, the surface displayed reversible changes in the Mn 2p_{3/2} position (Figure Sb-1), where at high potentials, the peak intensity of Mn IV was found to be larger than Mn III. The pristine $\alpha\text{-Mn}_2\text{O}_3$ spectrum was characterized by Mn 2p_{3/2} and Mn 2p_{1/2} transition at 641.3 and 653.0 eV, respectively. The deconvolution of the Mn 2p_{3/2} transition exhibited the presence of Mn III (641.6 eV) with a small shoulder in 640.6 eV assigned to Mn II (Figure 5c). After OER in 1 M KPi, the XP spectrum shifted reversibly toward higher binding energy tentatively interpreted as a partial oxidation of Mn II to Mn III (641.4) and Mn III to Mn IV (643.3) at the interface of the electrode (Figure 5c-1). The pristine Mn_3O_4 spectrum revealed a peak position of the Mn 2p_{3/2} and Mn 2p_{1/2} at 641.0 and 652.8 eV, respectively. The mixed valence compound^{50,53,59} was confirmed by deconvolution of the Mn 2p_{3/2} transition, where peaks at 640.2 eV (Mn II) and 641.5 eV (Mn III) were identified. In addition, a small shoulder in the Mn 2p_{3/2} transition at 639.3 eV was also observed and attributed to an impurity in the metal oxide (Figure 5d).^{54,60} After OER in 1 M KPi, Mn 2p_{3/2} transitions were shifted irreversibly to higher values, where Mn II and Mn 0 oxidized to Mn III (641.7 eV) and Mn IV (642.7 eV) (Figure 5d-1). In alkaline solution, $\alpha\text{-Mn}_2\text{O}_3$ and Mn_3O_4 displayed irreversible oxidation toward Mn III and Mn IV after changing the applied potential from voltages above and below the threshold value for oxygen evolution (SI, Figure S14); however, MnO_x -573 K exhibited the presence of Mn II even at high potential. This effect is not clear, but could be due to the presence of a certain region not oxidized as reported by Gorlin et al. where 20% of the film displayed lower oxidation states.⁶¹

The O 1s peak in MnO_x -373 K, $\alpha\text{-Mn}_2\text{O}_3$, and Mn_3O_4 films displayed the presence of Mn–O–Mn typical for manganese oxides, and a small peak belonging to a Mn–OH bonding. In the case of MnO_x -573 K, the broadness of the Mn 2p_{3/2} transition and the enlarged intensity of the Mn–OH peak was related to an increased number of chemical bonds⁶² probably available by changes in the active surface area or surface chemistry of MnO_x -573 K in agreement with the capacity measurements. After electrochemical evaluation in neutral solution, the peak of Mn–OH increased in all electrodes with respect to the Mn–O–Mn peak, especially in the case of $\alpha\text{-Mn}_2\text{O}_3$ and Mn_3O_4 , but remained unchanged for MnO_x -573, where structural water and carbonate (O 1s at 535 eV⁶³ and C 1s at 287.4 eV⁶⁴) were detected (Figure 6). In alkaline solution (SI, Figure S15), a similar effect was identified; however, MnO_x -573 K again displayed the presence of carbonate at higher potentials. Furthermore, at low potential, the O 1s most intense peak surprisingly shifted to 532.2 eV, which could be due to a shift in the Mn–O–Mn peak or possibly the presence of C–OH (also present in the C 1s spectra at 285.7 eV⁶⁵) (SI, Figure S16). Potassium incorporation from both electrolytes was also detected in MnO_x -573 K films. In general, the behavior observed during the electrochemical treatment of the electrode could be explained in a simplified model by the reaction of holes and OH groups with oxygen defects on the surface of the $\alpha\text{-Mn}_2\text{O}_3$ and MnO_x -573 K electrodes as shown in Figure 7.^{53,57,66}

In this simplified schematic representation (Figure 7), it is thought that oxygen vacancies present in the manganese oxide films and responsible for the decreased lattice constant in Mn_2O_3 and Mn_3O_4 possibly reacted at the electrode–

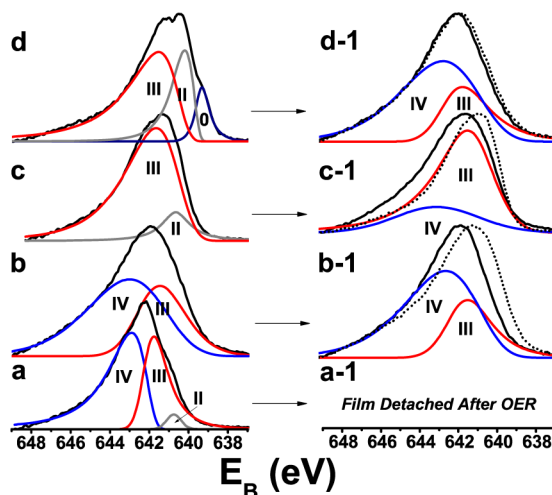


Figure 5. Deconvoluted XP spectra of Mn 2p_{3/2} before electrochemistry for MnO_x -373 K (a), MnO_x -573 K (b), $\alpha\text{-Mn}_2\text{O}_3$ (c), and Mn_3O_4 (d) films deposited on F:SnO₂/glass. Deconvoluted XP spectra after OER (at ~1.8 V vs RHE in 1 M KPi) for MnO_x -573 K (b-1), $\alpha\text{-Mn}_2\text{O}_3$ (c-1), Mn_3O_4 (d-1) films and treatment at ~1.1 V vs RHE (dotted line). Reversible changes found in $\alpha\text{-Mn}_2\text{O}_3$ and MnO_x -573 K.

possible due to the instability of the film. When the amorphous MnO_x -373 K films were heated at 573 K, the spectrum displayed a broad Mn 2p_{3/2} peak that when deconvoluted displayed the presence of Mn IV (643.0 eV) and Mn III (641.4 eV) and no longer the existence of Mn II. It is thought that the as deposited layers were present as $\text{Mn}(\text{OH})_2$, where manganese possessed an oxidation state of Mn II. After a heat treatment at 373 K, $\text{Mn}(\text{OH})_2$ was mainly converted to MnOOH and partially also to MnO_2 ; thus, leading to an

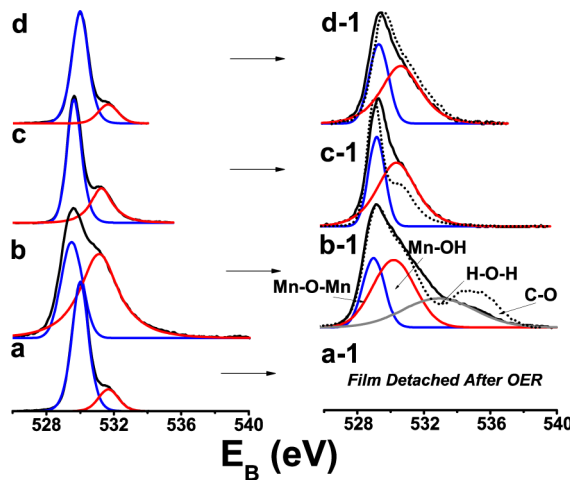


Figure 6. Deconvoluted XP spectra of O 1s before electrochemistry for MnO_x-373 K (a), MnO_x-573 K (b), α-Mn₂O₃ (c), and Mn₃O₄ (d) films deposited on F:SnO₂/glass. Deconvoluted XP spectra after OER (at ~ 1.8 V vs RHE in 1 M KPi) for MnO_x-573 K (b-1), α-Mn₂O₃ (c-1), Mn₃O₄ (d-1) films and treatment at ~ 1.1 V vs RHE (dotted line). Reversible changes found in α-Mn₂O₃ and MnO_x-573 K.

electrolyte interface with hydroxide ions from the electrolyte. As soon as the anodic potential reached the oxygen evolution reaction, the electrode surface reacted with holes generated by the applied positive potential; thus, forming oxygen gas and water molecules leaving behind oxygen vacancies and repeating the process again. Moreover, under OER conditions, the central Mn atoms in polyhedral coordination located close to the surface were oxidized from Mn^z to Mn^{z+1}.

The superior catalytic behavior of α-Mn₂O₃ was associated with its complex crystal structure. As mentioned before, α-Mn₂O₃ or C-type sesquioxide with orthorhombic symmetry crystallizes in a distorted bixbyite structure.^{29–32} One of the distinctive features of α-Mn₂O₃ is that MnO₆ octahedra can share 12 edges and six corners with neighboring coordination units. Furthermore, α-Mn₂O₃ possesses two different types of coordination octahedra. Type I octahedra (Mn in the Wyckoff position 4(a) and 4(b)) shows three pairs of Mn–O distances varying from 1.955 to 2.067 Å and in type II octahedra (three Mn atoms in Wyckoff position 8(c)) all distances are different, four short Mn–O bonds are located in a common plane with values ranging from 1.875 to 2.011 Å and two long bonds are found at each side of this plane forming the top of an elongated octahedron with distances varying from 2.192 to 2.306 Å.³² Compared to all other oxides summarized in Table S3, α-

Mn₂O₃ exhibits a very short O–O distance of 2.55 Å, which could facilitate the O₂ generation from these sites. In the case of MnO_x-573 K, such phase displayed comparable electrochemical results to α-Mn₂O₃, where the presence of slight crystallinity detected by Raman, could be responsible for the surface changes observed by XPS. Furthermore, distorted octahedra were also expected to be present with a valence state close to IV (similar to photosystem II)⁶⁷ since amorphous MnOOH and MnO₂ films are known to have high structural disorder, which could evoke to a variety of different Mn–O and Mn–OH bond distances. Therefore, it could be argued that the catalytic activity of MnO_x-573 K was also associated with its structural disorder.⁶⁸

In the case of Mn₃O₄, this phase shows semicovalent character in tetrahedral sites (Mn II occupancy with Mn–O distance of 1.812 Å) and in the apical bonds of octahedral sites (Mn III occupancy with Mn–O lengths of 2.386 Å). Furthermore, the remaining bonds of the octahedra display ionic character with a Mn–O length of 2.977 Å.⁶⁹ The observed distortion in the octahedra found in both phases can be explained by a Jahn–Teller effect due to the d⁴ state of the Mn III atoms in high spin configuration.^{23,33,70} Compared to Mn₃O₄, α-Mn₂O₃ presents a large variety in bond lengths; thus, offering a wide range of different Mn–O distances in the multistep process of water cleavage and oxygen formation. A further advantage of α-Mn₂O₃ is its low specific resistivity observed in capacity measurements (SI, Figure S7), where capacity was charged faster than in the other manganese oxides here evaluated (SI, Figure S5–S8). Reported values also showed similar tendencies, where α-Mn₂O₃ with $\rho = 5.3\text{--}8.0 \Omega \text{ cm}$ ⁶⁶ was lower than Mn₃O₄ ($\rho = 1.6 \times 10^2 \Omega \text{ cm}$)⁴⁷ and other manganese oxides such as, phyllosilicates (birnessite), and CaMn₂O₄ (marokite), which have values ranging from $\rho = 10^4$ to $10^8 \Omega \text{ cm}$.^{70,71} The combination of all these factors discussed above obviously played a crucial role in the performance of a prominent OEC electrocatalyst.

4. CONCLUSION

Galvanostatic anodic deposition was found to be a simple and efficient technique to prepare homogeneous films of nearly amorphous manganese oxide. Heat treatment of the films at 373 K was found to maintain the amorphous structure; however, at 573 K (although amorphous at first glance by X-ray diffraction) introduced a slight crystallization (detected by Raman Spectroscopy) and surface chemistry changes (identified by XPS). Further annealing at 773 K (under air) and 873 K (under N₂) led to a conversion into the crystallized phases of α-

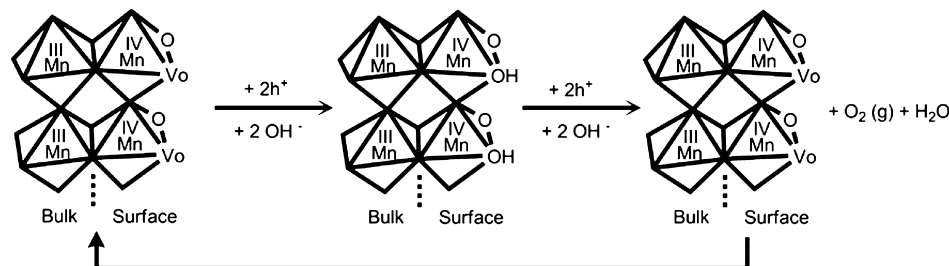


Figure 7. Schematic representation of manganese oxide octahedra (belonging to the bulk) and the surface interaction with the electrolyte (under anodic potential). The model assumes the presence of oxygen vacancies in MnO_x-573 K and α-Mn₂O₃ at the oxide electrolyte interface. In a first step, negatively charged oxygen defects react with holes and OH groups. In a second step, further holes and OH groups react with OH ions now occupying regular lattice sites of the oxides under formation of O₂ gas and a water molecule.

Mn_2O_3 and Mn_3O_4 , respectively. Electrochemical evaluation revealed that $\alpha\text{-Mn}_2\text{O}_3$ (mostly Mn III) films showed the smallest onset potential, i.e. the smallest overvoltage and highest current density related to the applied voltage followed closely by MnO_x -573 K (Mn III, IV) and the least active catalyst Mn_3O_4 (Mn II, III). These results led us to conclude that highest catalytic activity toward the oxygen evolution reaction was connected with the presence of Mn III ions in a distorted lattice, structural disorder (e.g., oxygen point defects) and a high variety of Mn–O bonds distances. The found overvoltages for $\alpha\text{-Mn}_2\text{O}_3$ were similar to pure NiO_x and NiCeO_x catalysts;⁷² thus, it can be expected that this manganese oxide could further improve in conductivity and therefore decrease its OER overvoltage.

ASSOCIATED CONTENT

Supporting Information

DEMS set up, X-ray diffraction of RuO_2 electrode, Raman spectroscopy, capacity measurements, CV measurements, and tables containing structural parameters and XPS values. This material is available free of charge via the Internet at <http://pubs.acs.org>.

AUTHOR INFORMATION

Corresponding Authors

(A.R.) E-mail: Alejandra.ramirez-caro@helmholtz-berlin.de.
(S.F.) E-mail: Fiechter@helmholtz-berlin.de.

Author Contributions

The manuscript was written through contributions of all authors. All authors have given approval to the final version of the manuscript.

Notes

The authors declare no competing financial interest.

ACKNOWLEDGMENTS

The authors would like to thank Dr. S. Brunken for the sputtered RuO_2 electrode, Dr. J. Rappich for the use of the Raman equipment, and Mrs. Ulrike Bloeck for TEM sample preparation and images. This work was supported by the German Federal Ministry of Education and Research (BMBF) under Contract #03SF0353A “H₂-NanoSolar”.

REFERENCES

- (1) Maeda, K.; Xiong, A.; Yoshinaga, T.; Ikeda, T.; Sakamoto, N.; Hisatomi, T.; Takashima, M.; Lu, D.; Kanehara, M.; Setoyama, T.; et al. Photocatalytic Overall Water Splitting Promoted by Two Different Cocatalysts for Hydrogen and Oxygen Evolution under Visible Light. *Angew. Chem., Int. Ed.* **2010**, *49*, 4096–4099.
- (2) Reece, S. Y.; Hamel, J. A.; Sung, K.; Jarvi, T. D.; Esswein, A. J.; Pijpers, J. J. H.; Nocera, D. G. Wireless Solar Water Splitting Using Silicon-Based Semiconductors and Earth-Abundant Catalysts. *Science* **2011**, *334*, 645–648.
- (3) Ramírez, A.; Bogdanoff, P.; Friedrich, D.; Fiechter, S. Synthesis of $\text{Ca}_2\text{Mn}_3\text{O}_8$ Films and Their Electrochemical Studies for the Oxygen Evolution Reaction (OER) of Water. *Nano Energy* **2012**, *1*, 282–289.
- (4) Dau, H.; Haumann, M. The Manganese Complex of Photosystem II in Its Reaction Cycle—Basic Framework and Possible Realization at the Atomic Level. *Coord. Chem. Rev.* **2008**, *252*, 273–295.
- (5) Siegbahn, P. E. M. Structures and Energetics for O_2 Formation in Photosystem II. *Acc. Chem. Res.* **2009**, *42*, 1871–1880.
- (6) Manickam, M.; Singh, P.; Issa, T. B.; Thurgate, S.; De Marco, R. Lithium Insertion into Manganese Dioxide Electrode in MnO_2/Zn Aqueous Battery: Part I. A Preliminary Study. *J. Power Sources* **2004**, *130*, 254–259.
- (7) Thackeray, M. Manganese Oxides for Lithium Batteries. *Prog. Solid State Chem.* **1997**, *25*, 1–71.
- (8) Brousse, T.; Long, J. W. Manganese Oxides: Battery Materials Make the Leap to Electrochemical Capacitors. *Electrochem. Soc. Interface* **2008**, *17*, 49–52.
- (9) Jeong, Y. U.; Manthiram, A. Nanocrystalline Manganese Oxides for Electrochemical Capacitors with Neutral Electrolytes. *J. Electrochem. Soc.* **2002**, *149*, A1419–A1422.
- (10) Devaraj, S.; Munichandraiah, N. High Capacitance of Electro-deposited MnO_2 by the Effect of a Surface-Active Agent. *Electrochim. Solid-State Lett.* **2005**, *8*, A373.
- (11) Chang, J.-K.; Tsai, W.-T. Material Characterization and Electrochemical Performance of Hydrous Manganese Oxide Electrodes for Use in Electrochemical Pseudocapacitors. *J. Electrochim. Soc.* **2003**, *150*, A1333–A1338.
- (12) Nam, K.-W.; Kim, M. G.; Kim, K.-B. In Situ Mn K-Edge X-ray Absorption Spectroscopy Studies of Electrodeposited Manganese Oxide Films for Electrochemical Capacitors. *J. Phys. Chem. C* **2007**, *111*, 749–758.
- (13) Xia, H.; Meng, Y. S.; Li, X.; Yuan, G.; Cui, C. Porous Manganese Oxide Generated from Lithiation/Delithiation with Improved Electrochemical Oxidation for Supercapacitors. *J. Mater. Chem.* **2011**, *21*, 15521–15526.
- (14) Lin, J.-C.; Chen, J.; Suib, S. L.; Cutlip, M. B.; Freihaut, J. D. Recovery of Bromine from Methyl Bromide Using Amorphous MnO_x Photocatalysts. *J. Catal.* **1996**, *161*, 659–666.
- (15) Cadus, L. E.; Ferretti, O. Characterization of Mo-MnO Catalyst for Propane Oxidative Dehydrogenation. *Appl. Catal. Gen.* **2002**, *233*, 239–253.
- (16) Gandía, L.; Vicente, M.; Gil, A. Complete Oxidation of Acetone over Manganese Oxide Catalysts Supported on Alumina- and Zirconia-Pillared Clays. *Appl. Catal. B Environ.* **2002**, *38*, 295–307.
- (17) Liu, Y.; Wei, Z.; Feng, Z.; Luo, M.; Ying, P.; Li, C. Oxidative Destruction of Chlorobenzene and O-Dichlorobenzene on a Highly Active Catalyst: $\text{MnO}_x/\text{TiO}_2-\text{Al}_2\text{O}_3$. *J. Catal.* **2001**, *202*, 200–204.
- (18) Gorlin, Y.; Jaramillo, T. F. A Bifunctional Nonprecious Metal Catalyst for Oxygen Reduction and Water Oxidation. *J. Am. Chem. Soc.* **2010**, *132*, 13612–13614.
- (19) Morita, M.; Iwakura, C.; Tamura, H. The Anodic Characteristics of Manganese Dioxide Electrodes Prepared by Thermal Decomposition of Manganese Nitrate. *Electrochim. Acta* **1977**, *22*, 325–328.
- (20) El-Deab, M. S.; Awad, M. I.; Mohammad, A. M.; Ohsaka, T. Enhanced Water Electrolysis: Electrocatalytic Generation of Oxygen Gas at Manganese Oxide Nanorods Modified Electrodes. *Electrochim. Commun.* **2007**, *9*, 2082–2087.
- (21) Harriman, A.; Pickering, I. J.; Thomas, J. M.; Christensen, P. A. Metal Oxides as Heterogeneous Catalysts for Oxygen Evolution under Photochemical Conditions. *J. Chem. Soc. Faraday Trans. 1* **1988**, *84*, 2795–2806.
- (22) Jiao, F.; Frei, H. Nanostructured Cobalt and Manganese Oxide Clusters as Efficient Water Oxidation Catalysts. *Energy Environ. Sci.* **2010**, *3*, 1018.
- (23) Robinson, D. M.; Go, Y. B.; Mui, M.; Gardner, G.; Zhang, Z.; Mastrogiovanni, D.; Garfunkel, E.; Li, J.; Greenblatt, M.; Dismukes, G. C. Photochemical Water Oxidation by Crystalline Polymorphs of Manganese Oxides: Structural Requirements for Catalysis. *J. Am. Chem. Soc.* **2013**, *135*, 3494–3501.
- (24) Yang, J.; Xu, J. J. Nanoporous Amorphous Manganese Oxide as Electrocatalyst for Oxygen Reduction in Alkaline Solutions. *Electrochim. Commun.* **2003**, *5*, 306–311.
- (25) Lee, J.-S.; Lee, T.; Song, H.-K.; Cho, J.; Kim, B.-S. Ionic Liquid Modified Graphene Nanosheets Anchoring Manganese Oxide Nanoparticles as Efficient Electrocatalysts for Zn–Air Batteries. *Energy Env. Sci.* **2011**, *4*, 4148–4154.
- (26) Zhou, F.; Izgorodin, A.; Hocking, R. K.; Armel, V.; Spiccia, L.; Macfarlane, D. R. Improvement of Catalytic Water Oxidation on MnO_x Films by Heat Treatment. *ChemSusChem* **2013**, *6*, 643–651.
- (27) Wu, M.-S.; Chiang, P.-C. J.; Lee, J.-T.; Lin, J.-C. Synthesis of Manganese Oxide Electrodes with Interconnected Nanowire Structure

- as an Anode Material for Rechargeable Lithium Ion Batteries. *J. Phys. Chem. B* **2005**, *109*, 23279–23284.
- (28) Chen, W.; Wang, N.; Liu, L.; Cui, Y.; Cao, X.; Chen, Q.; Guo, L. Facile Synthesis of Manganite Nanowires: Phase Transitions and Their Electrocatalysis Performance. *Nanotechnology* **2009**, *20*, 445601.
- (29) Cockayne, E.; Levin, I.; Wu, H.; Llobet, A. Magnetic Structure of Bixbyite α -Mn₂O₃: A Combined DFT+U and Neutron Diffraction Study. *Phys. Rev. B* **2013**, *87*, 184413.
- (30) Wyckoff, R. W. G. *Crystal Structures*, 2nd ed.; John Wiley & Sons, Inc.: New York, 1964; Vol. 2.
- (31) Geller, S. Structure of α -Mn₂O₃, (Mn_{0.983}Fe_{0.017})₂O₃ and (Mn_{0.37}Fe_{0.63})₂O₃ and Relation to Magnetic Ordering. *Acta Crystallogr. B* **1971**, *27*, 821–828.
- (32) Norrestam, R.; Ingri, N.; Östlund, E.; Bloom, G.; Hagen, G. Alpha-Manganese(III) Oxide — A C-Type Sesquioxide of Orthorhombic Symmetry. *Acta Chem. Scand.* **1967**, *21*, 2871–2884.
- (33) Baron, V.; Gutzmer, J.; Rundlof, H.; Tellgren, R. American Mineralogist. *Am. Mineral.* **1998**, *83*, 786–793.
- (34) Satomi, K. Oxygen Positional Parameters of Tetragonal Mn₃O₄. *J. Phys. Soc. Jpn.* **1961**, *16*, 258–266.
- (35) Ramírez, A.; Friedrich, D.; Kunst, M.; Fiechter, S. Charge Carrier Kinetics in MnO_x, Mn₂O₃ and Mn₃O₄ Films for Water Oxidation. *Chem. Phys. Lett.* **2013**, *568–569*, 157–160.
- (36) Bogdanoff, P.; Alonso-Vante, N. A Kinetic Approach of Competitive Photoelectrooxidation of HCOOH and H₂O on TiO₂ Anatase Thin Layers via On-Line Mass Detection. *J. Electroanal. Chem.* **1994**, *379*, 415–421.
- (37) Bogdanoff, P.; Alonso-Vante, N. *Ber. Bunsenges. Phys. Chem.* **1993**, *97*, 940–942.
- (38) Shinomiya, T.; Gupta, V.; Miura, N. Effects of Electrochemical-Deposition Method and Microstructure on the Capacitive Characteristics of Nano-Sized Manganese Oxide. *Electrochim. Acta* **2006**, *51*, 4412–4419.
- (39) Can Wang; Cheng, B. L.; Wang, S. Y.; Lu, H. B.; Zhou, Y. L.; Chen, Z. H.; Yang, G. Z. Effects of Oxygen Pressure on Lattice Parameter, Orientation, Surface Morphology and Deposition Rate of (Ba_{0.02}Sr_{0.98})TiO₃ Thin Films Grown on MgO Substrate by Pulsed Laser Deposition. *Thin Solid Films* **2005**, *485*, 82–89.
- (40) Fekete, M.; Hocking, R. K.; Chang, S. L. Y.; Italiano, C.; Patti, A. F.; Arena, F.; Spiccia, L. Highly Active Screen-Printed Electrocatalysts for Water Oxidation Based on β -Manganese Oxide. *Energy Environ. Sci.* **2013**, *6*, 2222–2232.
- (41) Najafpour, M. M. Conversions of Mn Oxides to Nanolayered Mn Oxide in Electrochemical Water Oxidation at near Neutral pH, All to a Better Catalyst: Catalyst Evolution - Dalton Transactions (RSC Publishing). *Dalton Trans.* **2013**, *42*, 16683–16686.
- (42) Julien, C. M.; Massot, M. Raman Spectroscopic Studies of Lithium Manganates with Spinel Structure. *J. Phys.: Condens. Matter* **2003**, *15*, 3151–3162.
- (43) Taylor, L. S.; Zografi, G. The Quantitative Analysis of Crystallinity Using FT-Raman Spectroscopy. *Pharm. Res.* **1998**, *15*, 755–761.
- (44) Gao, T.; Glerup, M.; Krumeich, F.; Nesper, R.; Fjellvåg, H.; Norby, P. Microstructures and Spectroscopic Properties of Cryptomelane-Type Manganese Dioxide Nanofibers. *J. Phys. Chem. C* **2008**, *112*, 13134–13140.
- (45) Julien, C.; Massot, M.; Baddour-Hadjean, R.; Franger, S.; Bach, S.; Pereira-Ramos, J. P. Raman Spectra of Birnessite Manganese Dioxides. *Solid State Ion.* **2003**, *159*, 345–356.
- (46) Shah, A. V.; Schade, H.; Vanecek, M.; Meier, J.; Vallat-Sauvain, E.; Wyrsch, N.; Kroll, U.; Droz, C.; Bailat, J. Thin-Film Silicon Solar Cell Technology. *Prog. Photovolt. Res. Appl.* **2004**, *12*, 113–142.
- (47) Dubal, D. P.; Dhawale, D. S.; Salunkhe, R. R.; Fulari, V. J.; Lokhande, C. D. Chemical Synthesis and Characterization of Mn₃O₄ Thin Films for Supercapacitor Application. *J. Alloys Compd.* **2010**, *497*, 166–170.
- (48) Audi, A. A.; Sherwood, P. M. A. Valence-Band X-ray Photoelectron Spectroscopic Studies of Manganese and Its Oxides Interpreted by Cluster and Band Structure Calculations. *Surf. Interface Anal.* **2002**, *33*, 274–282.
- (49) Di Castro, V.; Polzonetti, G. XPS Study of MnO Oxidation. *J. Electron Spectrosc. Relat. Phenom.* **1989**, *48*, 117–123.
- (50) Oku, M.; Hirokawa, K.; Ikeda, S. X-ray Photoelectron Spectroscopy of Manganese–Oxygen Systems. *J. Electron Spectrosc. Relat. Phenom.* **1975**, *7*, 465–473.
- (51) Foord, J. S.; Jackman, R. B.; Allen, G. C. An X-ray Photoelectron Spectroscopic Investigation of the Oxidation of Manganese. *Philos. Mag. A* **1984**, *49*, 657–663.
- (52) Zhao, Y.; Li, C.; Li, F.; Shi, Z.; Feng, S. One-Step Synthesis of Highly Water-Dispersible Mn₃O₄ Nanocrystals. *Dalton Trans.* **2010**, *40*, 583–588.
- (53) Chigane, M.; Ishikawa, M. Manganese Oxide Thin Film Preparation by Potentiostatic Electrolyses and Electrochromism. *J. Electrochem. Soc.* **2000**, *147*, 2246.
- (54) Moulder, J. F.; Stickle, W. F.; Sobol, P. E. *Handbook of X-ray Photoelectron Spectroscopy*; Perkin-Elmer, Physical Electronics Division: Waltham, MA, 1993.
- (55) An, G.; Yu, P.; Xiao, M.; Liu, Z.; Miao, Z.; Ding, K.; Mao, L. Low-Temperature Synthesis of Mn₃O₄ Nanoparticles Loaded on Multi-Walled Carbon Nanotubes and Their Application in Electrochemical Capacitors. *Nanotechnology* **2008**, *19*, 275709.
- (56) Moses Ezhil Raj, A.; Victoria, S. G.; Jothy, V. B.; Ravidhas, C.; Wollschläger, J.; Suendorf, M.; Neumann, M.; Jayachandran, M.; Sanjeeviraja, C. XRD and XPS Characterization of Mixed Valence Mn₃O₄ Hausmannite Thin Films Prepared by Chemical Spray Pyrolysis Technique. *Appl. Surf. Sci.* **2010**, *256*, 2920–2926.
- (57) Sharma, R. K.; Rastogi, A. C.; Desu, S. B. Manganese Oxide Embedded Polypyrrole Nanocomposites for Electrochemical Supercapacitor. *Electrochim. Acta* **2008**, *53*, 7690–7695.
- (58) Xie, X.; Liu, W.; Zhao, L.; Huang, C. Structural and Electrochemical Behavior of Mn–V Oxide Synthesized by a Novel Precipitation Method. *J. Solid State Electrochem.* **2010**, *14*, 1585–1594.
- (59) Dorris, S. E.; Mason, T. O. Electrical Properties and Cation Valencies in Mn₃O₄. *J. Am. Ceram. Soc.* **1988**, *71*, 379–385.
- (60) Biesinger, M. C.; Payne, B. P.; Grosvenor, A. P.; Lau, L. W. M.; Gerson, A. R.; Smart, R. S. C. Resolving Surface Chemical States in XPS Analysis of First Row Transition Metals, Oxides and Hydroxides: Cr, Mn, Fe, Co, and Ni. *Appl. Surf. Sci.* **2011**, *257*, 2717–2730.
- (61) Gorlin, Y.; Lassalle-Kaiser, B.; Benck, J. D.; Gul, S.; Webb, S. M.; Yachandra, V. K.; Yano, J.; Jaramillo, T. F. In Situ X-ray Absorption Spectroscopy Investigation of a Bifunctional Manganese Oxide Catalyst with High Activity for Electrochemical Water Oxidation and Oxygen Reduction. *J. Am. Chem. Soc.* **2013**, *135*, 8525–8534.
- (62) Fairley, N. *CasaXPS Manual 2.3.15 Spectroscopy*; Casa Software Ltd: Teignmouth, U.K., 2009.
- (63) López, G. P.; Castner, D. G.; Ratner, B. D. XPS O 1s Binding Energies for Polymers Containing Hydroxyl, Ether, Ketone and Ester Groups. *Surf. Interface Anal.* **1991**, *17*, 267–272.
- (64) Xue, Y.; Wang, Z.; Wang, J.; Hu, C.; Xie, F.; Chen, D.; He, Z. Evidence of Carboxyl Modification of Hydrogen-Free Diamond-Like Carbon Films Assisted by Radio Frequency Plasma in Vacuum. *Int. Sch. Res. Not.* **2012**, *2012*, e963298.
- (65) Wang, L. K.; Chen, J. P.; Hung, Y.-T.; Shammas, N. K. *Heavy Metals in the Environment*; CRC Press: Boca Raton, FL, 2011.
- (66) Morita, M.; Iwakura, C.; Tamura, H. The Anodic Characteristics of Massive Manganese Oxide Electrode. *Electrochim. Acta* **1979**, *24*, 357–362.
- (67) Zaharieva, I.; Chernev, P.; Risch, M.; Klingan, K.; Kohlhoff, M.; Fischer, A.; Dau, H. Electrosynthesis, Functional, and Structural Characterization of a Water-Oxidizing Manganese Oxide. *Energy Environ. Sci.* **2012**, *5*, 7081–7089.
- (68) Chang, S. L. Y.; Singh, A.; Hocking, R. K.; Dwyer, C.; Spiccia, L. Nanoscale Structural Disorder in Manganese Oxide Particles Embedded in Nafion. *J. Mater. Chem. A* **2014**, *2*, 3730–3733.
- (69) Due to discrepancies in Baron et al. coordinates, Mn₃O₄ bond distances were remeasured using a structure built by crystal maker with

cell parameters given by Satomi et al., oxygen position from Baron et al., and the rest of the values were taken from Wyckoff.

(70) Hocking, R. K.; Brimblecombe, R.; Chang, L.-Y.; Singh, A.; Cheah, M. H.; Glover, C.; Casey, W. H.; Spiccia, L. Water-Oxidation Catalysis by Manganese in a Geochemical-like Cycle. *Nat. Chem.* **2011**, *3*, 461–466.

(71) Matsumoto, Y.; Sato, E. Electrocatalytic Properties of Transition Metal Oxides for Oxygen Evolution Reaction. *Mater. Chem. Phys.* **1986**, *14*, 397–426.

(72) McCrory, C. C. L.; Jung, S.; Peters, J. C.; Jaramillo, T. F. Benchmarking Heterogeneous Electrocatalysts for the Oxygen Evolution Reaction. *J. Am. Chem. Soc.* **2013**, *135*, 16977–16987.